11th International Symposium on Turbulence and Shear Flow Phenomena (TSFP11)
Southampton, UK, July 30 to August 2, 2019

ROUGHNESS-INDUCED TRANSITION PREDICTION OVER COMPLEX GEOMETRIES WITH LINEAR PARABOLIZED STABILITY EQUATIONS (LPSE)

Francis Lacombe
Department of Mechanical and Mechatronics Engineering
University of Waterloo
200 University Ave W, Waterloo, ON N2L 3G1
flacombe@uwaterloo.ca

Jean-Pierre Hickey
Department of Mechanical and Mechatronics Engineering
University of Waterloo
200 University Ave W, Waterloo, ON N2L 3G1
jean-pierre.hickey@uwaterloo.ca

ABSTRACT

The effect of surface roughness on the stability characteristics at transonic conditions is investigated using the parabolized stability equations (PSE). The PSE numerical framework is formulated in curvilinear coordinates and the base flow is computed directly from the laminar compressible Navier-Stokes equations. The effect of surface roughness is directly tied to the local boundary layer characteristics of the flow. These PSE-generated results are validated against a high-order Direct Numerical Simulation (DNS) of roughness-induced transition. We also demonstrate that the PSE are sufficiently accurate to be used in combination with more sophisticated approaches (DNS, DES or LES) in order to reduce the computation time including in complex flow situations featuring compressibility and boundary curvature.

INTRODUCTION

For aircraft manufacturers, friction is the sinew of war; delaying laminar-to-turbulent transition–even over a short distance–can lead to significant drag reduction and, thus, performance improvements. Transition is greatly affected by the presence of dents and dimples resulting from hinge lines or rivet heads on the skin surface. For this reason, it is often necessary to modify the design by moving these geometric features further downstream in order to extend the laminar region of the flow. For instance, the engine nacelle and inlet lip have to be machined separately in order to assure that the hinge line does not induce a premature transition to turbulence. Due to the complexity of the flow on a nacelle, which include effects due to compressibility, pressure gradients, and cross-flow induced transition, most Reynolds Averaged Navier-Stokes (RANS) transition models fail to accurately predict the transition line–especially in the presence of surface imperfections. To this end, we present a numerical framework based on the Parabolized Stability Equations (PSE) to study the roughness-induced transition in transonic flows over complex geometries. From a design perspective, (Campbell & Lynde, 2017) demonstrated that the linear stability theory (LST) and PSE accounted for a sufficiently high level of physic (compressibility, curvature, etc.) to be incorporated into a preliminary natural laminar flow design method (NLF).

There are typically two families of modal-stability-based transition models: *local* and *nonlocal* methods. The *local* stability analysis is carried at a specific position in the flow, by opposition to the *nonlocal* approach that take into account the evolution of perturbations along their path (Juniper *et al.*, 2014). Traditionally, the local approaches, such as the Linear Stability Theory (LST), of which the Orr-Sommerfeld equations (OSE) is most well-known, perform particularly well in incompressible flows over simple geometries. However, in realistic aeronautical flows, compressibility, pressure gradients, cross-flow and roughness effects promote premature transition and are no longer negligible. For this reason, nonlocal approaches, such as the Parabolized Stability Equations (PSE), have received considerable attention in the last decades. Hall (1983) was the first to study the evolution of Tollmien-Schlichting (T-S) waves through a set of parabolized stability equations. Itoh (1981) and Bertolotti (1990) extended PSE to account for the nonlinear interaction between a subset of eigenmodes. More recently, Kuehl *et al.* (2012) and Moyes *et al.* (2017) used the Nonlinear PSE (NPSE) approach to study the secondary instability of cross-flow in hypersonic conditions. Lozano-Durán *et al.* (2018) showed that NPSE are sufficiently accurate to be used as inflow boundary conditions for Direct Numerical Simulation (DNS) or Large Eddy Simulation (LES). In this way, it is possible to significantly reduce the size of the computation domain by modelling the pre-transitional region using a simple boundary condition supplied from the NPSE. Their work focused on an incompressible zero-pressure gradient boundary layer, without any curvature, roughness or compressibility effects.

The effect of distributed roughness on the transitional

characteristics of compressible boundary layer was recently investigated by (Suryanarayanan *et al.*, 2017) who revisited the concept of roughness-shielding to reduce the receptivity of large amplitude discrete roughness elements. Using an hybrid DNS-experimental approach, they found that the use of continuous flat roughness strips either upstream or downstream of surface imperfections had a beneficial effect on transition control. More recently, (Montero & Pinna, 2018) and (Hein *et al.*, 2018) investigated the effect of three-dimensional discrete roughness elements on hypersonic flows using different approaches; Montero focused on a modal stability theory while Hein used a non-modal approach.

In the present paper, we develop a framework to solve the Parabolized Stability Equations for roughness induced transition in transonic flows. The PSE framework is intended as an initial design tool which accounts for surface imperfections. A validation of the transitional predictions is made with a Direct Numerical Simulation of the equivalent setup; which allows for a direct assessment of this predictive tool.

NUMERICAL CONSIDERATIONS

The modal stability theory is a branch of fluid mechanics that was initially developed to study the evolution of small amplitude perturbations within a variety of flows. It relies on the decomposition of the flow quantities into a steady part $\overline{q}$ and an unsteady part q' such that: $q(\vec{x},t) = \overline{q}(\vec{x}) + q'(\vec{x},t)$. All modal-stability based models rely on the assumption that the perturbation vector q' takes the following form: $q'(\vec{x},t) = \hat{q}(\vec{x})\chi(\vec{x},t)$, where $\hat{q}$ and χ are the amplitude and phase functions. Depending on the chosen approach (LST, PSE, NPSE, BiGlobal, etc.), $\hat{q}$ and χ will have different definitions. In the case of the Linear PSE, we assume the following:

$$q' = \hat{q}(x,y)\exp\left[\int_0^x i\alpha(x)dx + i\beta z - i\omega t\right] \tag{1}$$

where α, β and ω are the stream-wise, span-wise and temporal wavenumbers.

In the present work, we propose a model based on the dimensionless laminar compressible Navier-Stokes equations in their non-conservative form. In theory, the base flow ($\overline{q}$) does not depend on q' and the origin of $\overline{q}$ has little importance; one could choose to use a standalone CFD solver, interpolate the velocity field from experimental data or simply solve a set of self-similar equations (Blasius, Falkner-Skan-Cooke, etc.). However, as the PSE are derived directly from the non-conservative governing equations (2a)-(2c), we chose to compute the base flow directly from these same equations for numerical consistency.

$$\frac{\partial u_i}{\partial x_i} = \frac{1}{T}\frac{DT}{Dt} - \frac{1}{P}\frac{Dp}{Dt} \tag{2a}$$

$$\rho\left[\frac{\partial u_i}{\partial t} + u_j\frac{\partial u_i}{\partial x_j}\right] = -\frac{\partial p}{\partial x_i} + \frac{1}{Re}\frac{\partial \tau_{ij}}{\partial x_j} \tag{2b}$$

$$\rho c_p\left[\frac{\partial T}{\partial t} + u_j\frac{\partial T}{\partial x_j}\right] = \frac{1}{RePr}\frac{\partial}{\partial x_i}\left(\lambda\frac{\partial T}{\partial x_i}\right) + (\gamma-1)M^2\left(u_i\frac{\partial p}{\partial x_i}\right) + \phi_{ij} \tag{2c}$$

The laminar base flow as well as the stability equations are solved using an hybrid approach by combining two types of numerical schemes. In the wall-normal direction, we use a spectral-collocation-based method to account for the steepest gradient of the solution. In the stream-wise direction, we use a central sixth-order finite-difference scheme which is better adapted for complex geometries than spectral collocations methods.

The spectral collocation method is well suited for the PSE approach and has been used by several other authors (Shen *et al.*, 2011; Bertolotti, 1992; Thomas *et al.*, 2017). The main idea is to expand the solution in terms of global basis functions so that the numerical solution satisfies the PDE at the so-called *collocation points*, or also named *Chebyshev Gauss-Lobatto points* (Hussaini *et al.*, 1989), defined as: $\xi_j = \cos\frac{\pi j}{n}$. In the present case however, to accurately capture the physic of the problem in the vicinity of the wall using a standard spectral collocation method, one would have to increase the polynomial order in the range of 100-200. At sufficiently high polynomial orders (in our experience around 200), the problem become poorly-conditioned and numerical error begins to propagate within the solution. To correct this behaviour, we use a multi-element spectral-collocation method consisting of multiple lower order collocation sub-domains. In this way, the problem can be elegantly discretized using the following differentiation matrices:

$$\mathscr{D} = \begin{bmatrix} \Phi_0 & 0 & 0 \\ 0 & \Phi_1 & 0 \\ 0 & 0 & \Phi_2 \end{bmatrix} \qquad \mathscr{D}^2 = \mathscr{D}\cdot\mathscr{D} \tag{3}$$

where Φ_i is the standard spectral differentiation matrix for the i^{th} sub-domain. In practice, this method is more robust, but also more efficient than standard collocation methods as the resulting differentiation matrix allows the use of sparse matrices and optimized sparse solvers such as Intel MKL Pardiso. We typically use eight twentieth-order sub-domains with a stronger nodes concentration at the wall which results in a sparsity index in the range of 0.875.

Using equation (3) and Backward Differentiation Formulas (BDF), the LPSE system can be written has:

$$\left[L + \mathscr{D}P + \mathscr{D}^2 S - E\frac{1}{\Delta x}\right]\vec{q}_i = -E\frac{1}{\Delta x}\vec{q}_{i-1} \tag{4}$$

where $\vec{q} = [\hat{u},\hat{v},\hat{w},\hat{p},\hat{T}]^T$, $\mathscr{D}$ is the differentiation matrix and the matrices L,P,S and E depend on the base flow and the wavenumbers only.

The stream-wise wave number α is x-dependant in PSE. An additional equation must then be added to close the system: this is the *normalization condition* (also called *auxiliary condition*) Juniper *et al.* (2014). The role of the normalization condition is to transfer energy from the amplitude function to the phase function such that $\partial_{xx}\vec{q} \sim O(Re_\delta^{-2})$.

$$\int_0^\infty \hat{q}^\dagger\frac{\partial\hat{q}}{\partial x}dy = 0 \tag{5}$$

The equations have been *parabolized* as we eliminated the second x-derivatives of $\vec{q}$. However, there is still some ellipticity present in the system, mostly due to the reverse propagation due to the pressure terms. The problem arises when

the step size become smaller than $\frac{1}{|\alpha_r|}$Li & Malik (1997). There are multiple ways to alleviate this constraint. The simplest way is to define a minimal lower bound on the marching step size. In practice, it is not always possible as complex geometries may require a smaller step size to accurately represent sharp edges. Alternatively, as shown by Li & Malik (1997), we can drop the $\frac{\partial \hat{p}}{\partial x}$ terms, in which case, the step size restriction is relaxed but not eliminated. Finally, it is also possible to add a stabilizing term to the system. For the first-order Euler scheme, the following expression can be derived:

$$\mathscr{L}\hat{q} + \mu\mathscr{L}\frac{\partial \vec{q}}{\partial x} = -\mathscr{B}\frac{\partial \vec{q}}{\partial x} \tag{6}$$

Once discretized:

$$\left[\mathscr{L} + \frac{\mu}{\Delta x}\mathscr{L}\right]\vec{q_i} = \left[\frac{\mathscr{B} - \mu\mathscr{L}}{\Delta x}\right]\vec{q_{i-1}} \tag{7}$$

where μ is defined as $\max(\frac{2}{|\alpha_r|} - 2\delta x, 0)$ and has the same order of magnitude as the truncation error associated with the first-order backward differentiation scheme. In other words, the final solution is not impacted by the stabilizing term.

RESULTS and DISCUSSIONS

In this section, we first conduct an analysis on a transitional subsonic boundary-layer using a modal stability approach (LPSE) as a baseline case. A representative roughness-induced transition case is then proposed and investigated using both PSE and DNS.

PSE results

As the linear PSE neglects all the non-linear coupling terms, the exact transition location must be estimated. The e^N method is widely used in aerodynamic design. Based on empirical measurements, colossal efforts have been deployed by the industry to collect the experimental data needed for the N-factor correlations Herbert (1997). By integrating the growth rate along the stream-wise direction, it is possible to obtain the *n-factor* defined as:

$$\text{n-factor} = -\int_{x_0}^{x_i} \sigma dx \tag{8}$$

The n-factor can be seen as a mode-specific measure of the disturbance amplification along the stream path. It should however be noted that the n-factor is a function of the temporal wavenumber (ω); thus, it can not be directly correlated to the transition position. To remove this ambiguity, Ingen (1956) defined the *N-factor* corresponding to the envelope of the n-factor curves (see figure 5). Ingen (2008) correlated the following critical N-factors for the beginning and end of transition in an incompressible flat plate boundary-layer as a function of the free-stream turbulence intensity. The beginning and end of transition are respectively: N

$$_B = 2.13 - 6.18\log_{10}(Tu) \tag{9a}$$
$$N_E = 5.00 - 6.18\log_{10}(Tu) \tag{9b}$$

It has been shown that the use of compressible linear stability theory to compute critical N-factors leads to larger scatter, then in the case of incompressible linear stability theory. However, Risius *et al.* (2018) found that this is generally not the case and that compressible critical N-factors, once corrected for the influence of the external disturbance spectrum, show a better correlation.

A zero-pressure gradient, smooth flat plate transitional boundary layer is investigated using the developed parabolized stability framework. A first case is investigated at the incompressible limit, given the well-studied nature of the incompressible boundary layer, as a validation of the framework. The neutral stability curve computed from PSE slightly underestimates the experimental stability bounds but collapses well with published DNS data as shown in Figure 1.

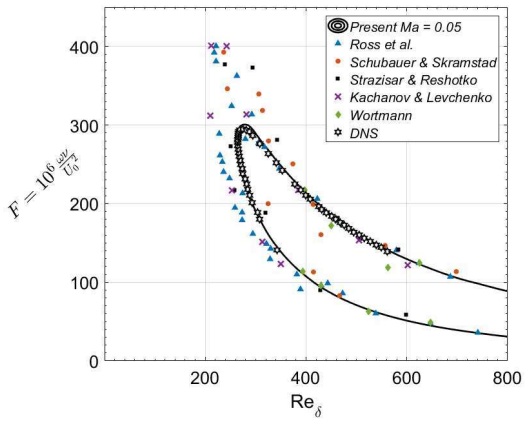

Figure 1. Neutral stability curve for an incompressible ZPG flat plate boundary layer, $Re_\delta = \sqrt{Ux/\nu}$

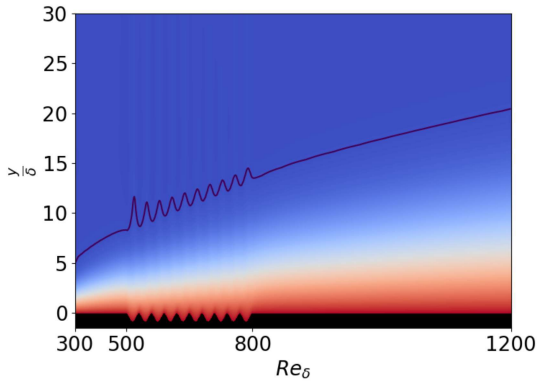

Figure 2. Velocity contour plot from the laminar solver; the boundary layer thickness $\delta_{0.99}$ is shown as a solid line. The y-axis is expanded for increased visibility of the roughness elements. The x-axis is not linear as the Reynolds number is based on the boundary layer thickness. The height of the roughness array corresponds to $\approx 0.16\delta_{0.99}$. Where $\delta_{0.99}$ is evaluated at the inlet.

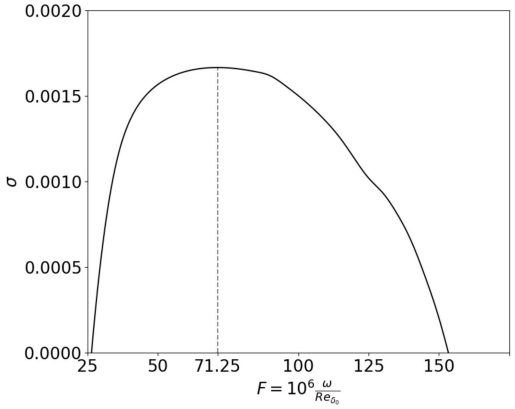

Figure 3. Maximum growth rate vs dimensionless frequency, for a compressible ZPG flat plate. $Ma = 0.7$, $Re_{\delta_0} = 300$, $\frac{T_{wall}}{T_\infty} = 1$

A roughness-induced transition of a compressible zero-pressure-gradient flat plate boundary layer at Mach 0.7 is investigated using the PSE framework. The setup consists of a flat plate to which we have added a roughness array of 10 successive sinusoidal humps (see figure 2). The inlet Reynolds number, $Re_{\delta_0} = \frac{u\delta_0}{\nu}$, is set to 300 based on a length scale which is proportional to the *inlet* boundary layer thickness, where $\delta = \sqrt{\frac{\nu x}{u}}$. The dimensionless height of the roughness array is approximately 16% of the inlet boundary layer thickness such that the roughness elements do not trigger a transition to turbulence, they instead cause a precocious transition downstream of the roughness array. To this end, the roughness array begins at $x/\delta_0 = 833$ and extends up to $x/\delta_0 = 2133$; this corresponds to a range from $Re_\delta = 500$ to 800. We determined the location of the roughness array based on the maximum growth rate of the most unstable mode (in the smooth configuration). The most unstable mode was determined by sweeping the frequency spectrum and finding the temporal frequency leading to the highest growth rate (see figure 3). The growth rate was computed using the LPSE approach from equation (10).

$$\sigma = -Im(\alpha) + \frac{\partial}{\partial x}\left[\ln\left(\sqrt{E_k}\right)\right] \tag{10}$$

$$E_k = \int_0^\infty \overline{\rho}\left(|\hat{u}|^2 + |\hat{v}|^2 + |\hat{w}|^2\right) dy \tag{11}$$

The neutral stability stability and N-factor curves of the roughness-induced transition are shown in figures 4 and 5, respectively. Two important observations are noted. First, the bounds of neutral stability are greatly increased, particularly around the roughness elements. Second, the growth of the instability modes are greatly enhanced compared to the smooth configuration.

DNS results

A DNS of the roughness-induced transitional configuration was conducted using the Nektar++ compressible solver Cantwell *et al.* (2015). For inflow boundary condition, we used a self-similar compressible Blasius profile to which we superimposed T-S waves with a prescribed amplitude. Since the T-S waves are computed from the linear sta-

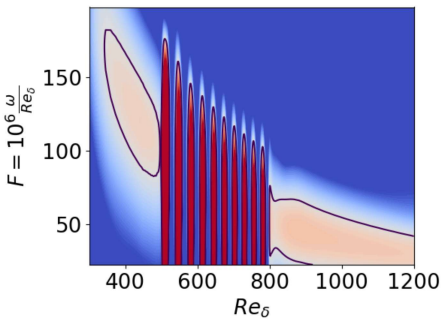

Figure 4. Neutral stability curve of roughness-induced transition at $Ma = 0.7$.

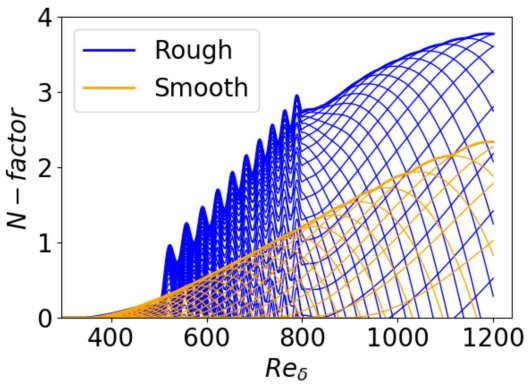

Figure 5. N-factor for the compressible boundary layer (Ma = 0.7)

bility theory, only the relative scaling between u', v', w', T' and p' has a physical meaning, the solution must thus be scaled to reflect the case of interest. In the present case, we impose a 0.6% turbulence intensity (Tu[%]) at the inlet:

$$\text{Tu}[\%] = \frac{u'}{u_{ref}} = \frac{1}{u_{ref}}\sqrt{\frac{u'^2}{3} + \frac{v'^2}{3} + \frac{w'^2}{3}} \tag{12}$$

Where u', v' and w' are the root mean square (RMS) fluctuating velocities. In the modal stability theory, the fluctuating flow is a sum of sinusoidal-type modes with a RMS amplitude given by :

$$u_i' = \frac{|\hat{u}_i|_{max}}{\sqrt{2}} \tag{13}$$

The scaling factor applied to $\hat{q}$ is thus chosen such that the $Tu[\%] = 0.6\%$ (see figure 6).

$$\text{Tu}[\%] = 0.006 = \frac{1}{u_{ref}}\sqrt{\frac{|\hat{u}|^2_{max}}{6} + \frac{|\hat{v}|^2_{max}}{6} + \frac{|\hat{w}|^2_{max}}{6}} \tag{14}$$

For the remaining boundary conditions, we use a pressure outflow and the laminar solution in the free-stream.

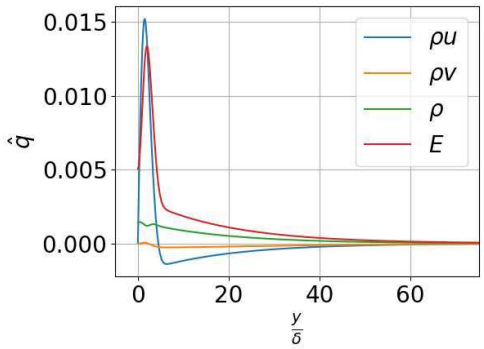

Figure 6. Perturbation vectors at $Re_\delta = 300$ computed from the compressible Linear Stability Theory (LST). The amplitude of the vector is chosen such that $Tu[\%] = 0.6\%$

The wall is kept at a constant temperature $\frac{T_{wall}}{T_\infty} = 1$ as for the PSE case. The grid converged solution required $1600 \times 640 \times 32$ degrees-of-freedom using a 3rd order polynomial. The near wall resolution was maintained below $y^+ = 0.1$. The streamwise resolution of the roughness elements was ≈ 460.

The process leading to the onset of turbulence generally occurs gradually over a relatively short distance; estimating a precise transition location is thus incoherent with the physical process. For instance, using the skin friction coefficient, the beginning and end of transition are usually assumed to be bounded by the local minimum and maximum wall shear stress respectively. As shown on the figure 7, the skin friction coefficient obtained by adding the time-averaged contribution of the primary disturbance mode to the laminar flow agrees well with the DNS results until transition is triggered. According to equations (9a) and (9b) and referring to figure 5, the transition process should begin slightly after $Re_\delta = 1000$ (based on the correlated N-factor of transition onset). According to the DNS results, the transition begins slightly before $Re_\delta = 1000$ which is surprisingly accurate considering that the critical N-factors were correlated for a perfectly smooth incompressible flat plate boundary-layer; the stabilizing effect of compressibility is to decrease the N-factor curves' amplitude rather than the critical N-factor values.

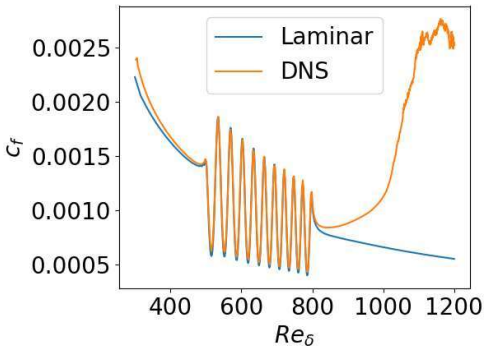

Figure 7. Skin friction coefficient obtained from the Laminar solver compared against Direct Numerical Simulations (DNS)

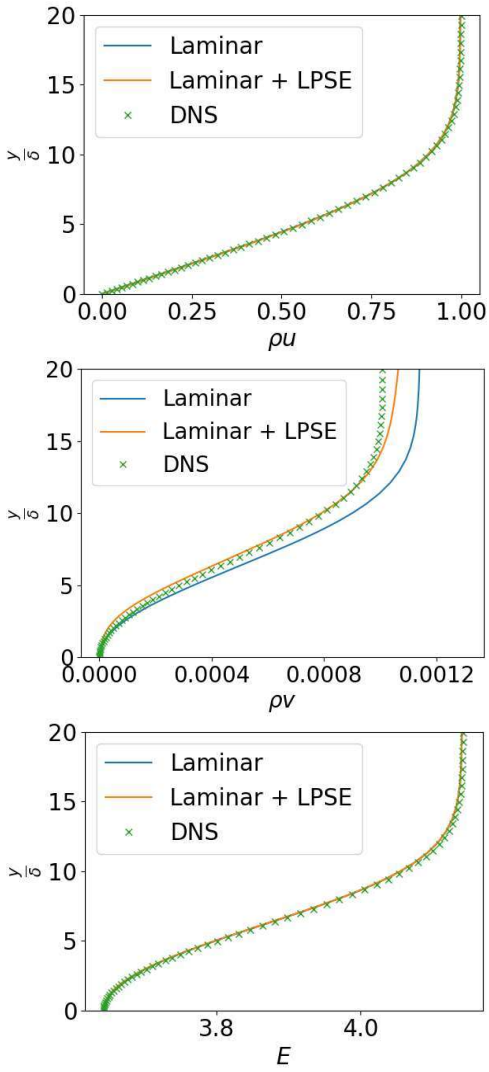

Figure 8. momentum and energy profiles downstream of the roughness array ($Re_\delta = 850$) at $t = 7461$

Figures 8 show a comparison of the instantaneous stream-wise/wall-normal momentum and energy profiles immediately after the roughness array. The linear PSE seems to adequately predict the evolution of the perturbation vectors even in presence of moderate surface roughness. The discrepancy observed in the free-stream wall-normal momentum can be tied to slight differences in the boundary conditions used in the laminar and LPSE solver compared to the DNS solver. First, the laminar and LPSE models are solved in a boundary-fitted coordinates and instead of using a pressure outflow boundary condition in the free-stream, we simply set the normal derivative to zero. Another significant difference is the viscosity model. In the laminar and LPSE solvers, we assume a variable viscosity based on the Sutherland's law while the DNS solver uses a constant viscosity assumption. Nonetheless, the cumulative effect of the roughness array on the flow stability was adequately predicted using the LPSE. Following the work of Lozano (Lozano-Durán *et al.*, 2018), it seems to be possible to replace the flow section containing the roughness elements by a simple time dependent Dirichlet boundary condition which could lead to significant CPU saving. To

provide an order of magnitude, the DNS took several days using 1600 CPUs on a high-performance computing cluster while the laminar and LPSE results were generated in just a few hours using 4 cores on a standard laptop.

CONCLUSION

Numerical studies of a compressible boundary-layer in a normal transition scenario (T-S waves) were conducted using both the Linear Parabolized Stability Equations (LPSE) and Direct Numerical Simulations (DNS). The transition prediction obtained from the classical e^N method agreed surprisingly well with the DNS, considering the fact that we used the incompressible critical N-factor. The momentum and energy profiles downstream of the roughness array predicted by the LPSE were in good agreement with the DNS, indicating that it could be used as time-dependent boundary condition for DNS, DES or LES in order to reduce the size of the computational domain.

Acknowledgment

This research was enabled in part by support provided by SciNet and Compute Canada. We acknowledge the support of the Natural Sciences and Engineering Research Council of Canada (NSERC).

REFERENCES

Bertolotti, Fabio 1990 The Effect of Approximations to the Thermodynamic Properties on the Stability of Compressible Boundary Layer Flow. In *Instability and Transition*, pp. 83–98. New York, NY: Springer New York.

Bertolotti, FP 1992 Linear and nonlinear stability of the Blasius boundary layer. *Journal of Fluid Mechanics* **242** (-1), 441–474.

Bertolotti, F. P. & Herbert, Th 1991 Analysis of the linear stability of compressible boundary layers using the PSE. *Theoretical and Computational Fluid Dynamics* **3** (2), 117–124.

Campbell, Richard L & Lynde, Michelle N 2017 Building a Practical Natural Laminar Flow Design Capability pp. 1–21.

Cantwell, Chris D, Moxey, David, Comerford, Andrew, Bolis, Alessandro, Rocco, Gabriele, Mengaldo, Gianmarco, De Grazia, Daniele, Yakovlev, Sergey, Lombard, J-E, Ekelschot, D *et al.* 2015 Nektar++: An open-source spectral/hp element framework. *Computer physics communications* **192**, 205–219.

Hall, P. 1983 The linear development of Gortler vortices in growing boundary layers. *Journal of Fluid Mechanics* **130**, 41–58.

Hein, Stefan J., Theiss, Alexander, Di Giovanni, Antonio, Stemmer, Christian, Schilden, Thomas, Schroeder, Wolfgang, Paredes, Pedro, Choudhari, Meelan M., Li, Fei & Reshotko, Eli 2018 Numerical Investigation of Roughness Effects on Transition on Spherical Capsules. In *2018 AIAA Aerospace Sciences Meeting*, pp. 1–25. Reston, Virginia: American Institute of Aeronautics and Astronautics.

Herbert, Thorwald 1997 Parabolized Stability Equations. *Annual Review of Fluid Mechanics* **29** (1), 245–283.

Hussaini, M. Y., Kopriva, D. A. & Patera, A. T. 1989 Spectral collocation methods. *Applied Numerical Mathematics* **5** (3), 177–208.

Ingen, J. L. van 1956 A suggested semi-empirical method for the calculation of the boundary layer transition region.

Ingen, J. L. Van 2008 Historical review of work at TU Delft. *38th Fluid Dynamics Conference and Exhibit* (June), 1–49.

Itoh, N. 1981 Secondary Instability of Laminar Flows. *Proceedings of the Royal Society A: Mathematical, Physical and Engineering Sciences* **375** (1763), 565–578.

Juniper, Matthew P., Hanifi, Ardeshir & Theofilis, Vassilios 2014 Modal Stability TheoryLecture notes from the FLOW-NORDITA Summer School on Advanced Instability Methods for Complex Flows, Stockholm, Sweden, 2013 ¡sup¿1¡/sup¿. *Applied Mechanics Reviews* **66** (2), 021004.

Kuehl, Joseph, Perez, Eduardo & Reed, Helen 2012 JoKHeR: NPSE Simulations of Hypersonic Crossflow Instability. *50th AIAA Aerospace Sciences Meeting including the New Horizons Forum and Aerospace Exposition* (January), 1–14.

Li, Fei & Malik, Mujeeb R. 1997 Spectral analysis of parabolized stability equations. *Computers and Fluids* **26** (3), 279–297.

Lozano-Durán, A., Hack, M. J.P. & Moin, P. 2018 Modeling boundary-layer transition in direct and large-eddy simulations using parabolized stability equations. *Physical Review Fluids* **3** (2).

Montero, Iván Padilla & Pinna, Fabio 2018 Stability Analysis of the Boundary Layer Developing on a Flat Plate with Discrete Roughness Elements in Hypersonic Flow (January).

Moyes, Alexander J., Paredes, Pedro, Kocian, Travis S. & Reed, Helen L. 2017 Secondary instability analysis of crossflow on a hypersonic yawed straight circular cone. *Journal of Fluid Mechanics* **812**, 370–397.

Risius, Steffen, Costantini, Marco, Koch, Stefan, Hein, Stefan & Klein, Christian 2018 Unit Reynolds number, Mach number and pressure gradient effects on laminar-turbulent transition in two-dimensional boundary layers. *Experiments in Fluids* **59** (5), 86.

Shen, Jie, Tang, Tao & Wang, Li-Lian 2011 *Spectral Methods*, *Springer Series in Computational Mathematics*, vol. 41. Berlin, Heidelberg: Springer Berlin Heidelberg.

Suryanarayanan, Saikishan, Goldstein, David B., Berger, Alexandre R., White, Edward B. & Brown, Garry L. 2017 Mechanics of Distributed Roughness Shielding for Suppression of Roughness Induced Boundary Layer Transition. *47th AIAA Fluid Dynamics Conference* (June), 1–17.

Thomas, Christian, Mughal, Shahid, Ashworth, Richard, Thomas, Christian, Mughal, Shahid & Ashworth, Richard 2017 On predicting receptivity to surface roughness in a compressible infinite swept wing boundary layer On predicting receptivity to surface roughness in a compressible infinite swept wing boundary layer **034102**, 1–30.

Tolieng, Vasana, Prasirtsak, Budsabathip, Sitdhipol, Jaruwan, Thongchul, Nuttha & Tanasupawat, Somboon 2017 Identification and lactic acid production of bacteria isolated from soils and tree barks. *Malaysian Journal of Microbiology* **13** (2), 100–108.